

Comparative Study of Experimental Choroidal Neovascularization by Optical Coherence Tomography and Histopathology

Toshio Fukuchi, Kanji Takahashi, Masanobu Uyama and Miyo Matsumura

Department of Ophthalmology, Kansai Medical University, Osaka, Japan

Purpose: To study the development, progression, and regression of experimental choroidal neovascularization (CNV) by correlating the cross-sectional images from sequential optical coherence tomography (OCT) with histopathologic sections of the same retinal regions.

Methods: Laser photocoagulation was performed in the posterior pole of the eye of 4 rhesus monkeys to induce CNV. Funduscopy, fluorescein angiography (FAG), and OCT were performed on day 1 and weekly for 13 weeks. Histological serial sections of CNV tissue were compared to corresponding OCT images.

Results: In the developmental stage of CNV, the CNV was observed by OCT as a nodular high reflex area continuing from the highly reflective retinal pigment epithelium (RPE). Histopathological studies showed that the CNV was composed of tightly packed proliferated RPE and immature vascular endothelial cells. In the active stage, OCT revealed a thick multi-layered high reflex area under the sensory retina. This high reflex area corresponded with the CNV membrane that consisted of newly formed blood vessels with wide vascular lumens and proliferated spindle-shaped RPE cells. In the regressive stage, OCT revealed a dome-like, white-colored highly reflective layer continuing from the RPE layer with moderate reflection beneath the layer. Histopathologically, the neovascular tissue was enveloped by mono-layered, cuboidal-shaped RPE cells with melanin granules.

Conclusion: Optical coherence tomography images clearly demonstrated the positional relationship between the CNV and the RPE. Optical coherence tomography imaging provides information on the CNV which complements conventional examinations by funduscopy and FAG. **Jpn J Ophthalmol 2001;45:252–258** © 2001 Japanese Ophthalmological Society

Key Words: Choroidal neovascularization, optical coherence tomography, retinal pigment epithelium.

Introduction

The use of optical coherence tomography (OCT) was initially reported by Huang et al in 1991.¹ Thereafter, OCT has been widely used in clinical practice^{2–6} as OCT facilitates a noninvasive observation of the fine tomographic features of the eye by utilizing the interference of light phenomenon. Prior to OCT, fluorescein angiography (FAG) and indocyanine-green angiography (ICG) were developed to supplement standard funduscopy to detect and diagnose ocular fundus diseases. It has been demon-

strated that these procedures were quite useful for detecting choroidal neovascularization (CNV).^{7,8} However, they were limited because it was difficult to evaluate the three-dimensional structure of the positional relationship between the CNV and the retinal pigment epithelium (RPE).

Examining the serial cross-sectional appearance of a tissue by OCT is useful to obtain a three-dimensional image of a structure. However, it has not been completely determined how the OCT images correlate with the histopathological studies of the same area.

In recent years, submacular surgery has been indicated for the CNV associated with age-related macular degeneration (AMD), and it is very important to identify the site of the CNV before the beginning of surgery. Gass has classified CNV into 2 types: type 1, in which the CNV originates from below the retinal

Received: June 19, 2000

Correspondence and reprint requests to: Kanji TAKAHASHI, MD, PhD, Department of Ophthalmology, Kansai Medical University, 10-15 Fumizoncho, Moriguchi, Osaka, 570-8507, Japan

pigment epithelium; and type 2, in which the CNV grows between the retina and the RPE.⁹ It has been shown that OCT provides tomographic images useful for differentiating between the two types of CNV.¹⁰⁻¹²

To obtain more information on the relationship of the OCT images to the actual structure, we induced experimental CNV by intense laser photocoagulation of monkey eyes. During the development, active progression, and regression of the experimental CNV, we examined the tomographic images of the neovascularization by OCT. Eyes were taken at critical times for histopathological study of the CNV and compared to the OCT images of the same sites.

Materials and Methods

Animals and Procedures

Four eyes of 4 adult rhesus monkeys, *Macaca irus*, ranging from 1.5 to 2.5 kg were used. The animals were used in accordance with federal regulations, the Care and Use of Animals (National Institutes of Health Publication No. 85-23), and the Association for Research in Vision and Ophthalmology Resolution on the Use of Animals in Ophthalmic and Vision Research.

After general anesthesia by an intramuscular injection of 25 mg/kg of ketamine hydrochloride, mydriasis was induced with topical 0.5% tropicamide and 0.5% phenylephrine hydrochloride. Using a Goldmann-type fundus contact lens, eight intense photocoagulation spots were made in grid pattern on the temporal and the nasal sides of the posterior pole of the fundus (16 spots per eye) with a krypton laser (System-910; Coherent, Palo Alto, CA, USA). A modification of Ryan's method was used.¹³

Funduscopy, FAG, and OCT (Zeiss-Humphrey, Dublin, CA, USA) were performed on the day after the photocoagulation and at 1-week intervals until 13 weeks after photocoagulation. All of the monkeys survived the experimental period (from 1 to 13 weeks) and did not appear to be visually impaired by the photocoagulation.

OCT Imaging

The center of the photocoagulation spots, including the surrounding normal tissue, was scanned by OCT at the times designated. The OCT system divided the reflection from retina into 256 steps, and coded the density of the tissue by the strength of reflection as white, red, yellow, green, blue, and black in decreasing levels of reflection. The mean scan length of the OCT was 2.41 mm (minimum, 1.17 mm; maximum, 4.03 mm). The OCT findings were com-

pared to the histopathological findings for the same lesion by detecting the rupture of Bruch's membrane under a light microscope.

Histopathological Preparations

Enucleation was performed at 1 week after photocoagulation as well as at 2, 4, and 13 weeks after photocoagulation. One eye was used for each time point.

The eyes were prefixed in 4% glutaraldehyde in 0.1 M phosphate buffer for 24 hours, washed in 0.1 M phosphate buffer, and postfixed in 1% osmium tetroxide phosphate buffer.

The specimens were dehydrated in a graded series of ethanol and the ethanol was replaced by propylene oxide before embedding in epon 812. Using a microtome, 2- μ m serial sections were cut. After toluidine blue staining, the photocoagulation site was examined under a light microscope (BH-2; Olympus, Tokyo).

Results

After photocoagulation, CNV developed in 30 of the 64 (46.9%) coagulation spots. In 29 (96.7%) of these spots, CNV occurred within 2 weeks after photocoagulation. All but four of the CNV areas became confluent with adjacent CNV and were of 1 disc diameter or smaller. Thereafter, 10 spots showed spontaneous regression. In 1 rhesus monkey that was followed for 13 weeks after photocoagulation, 8 (66.7%) of the 12 CNV showed complete regression within 10 weeks after photocoagulation.

Stages of CNV

Based on funduscopy and FAG findings, the CNV were classified into the developmental stage, active stage, and regressive stage. The CNV at the developmental stage occurred within 2 weeks after photocoagulation and showed hyperfluorescence from early to late phase of FAG. There was no dye leakage at this stage. The CNV at the active stage appeared ophthalmoscopically grayish-white with irregular border under the retina and showed marked leakage of fluorescein during the late phase of FAG. The CNV at the regressive stage appeared dark-brown with slight pigmentation and showed no leakage during the late phase.

Basic OCT Pattern and Histopathological Findings at Each Stage

Developmental stage of CNV. During the developmental stage, round, grayish-white subretinal lesions were seen in the photocoagulated sites by oph-

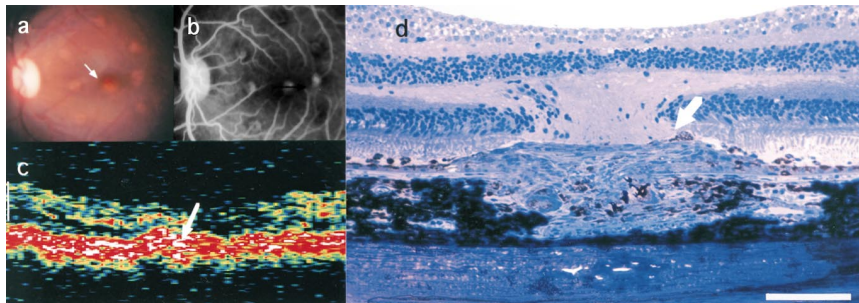


Figure 1. Developmental stage of choroidal neovascularization (CNV), 1 week after photocoagulation. **(a)** Color fundus photograph. Coagulated spot appears as grayish-white lesion. Coagulated spot indicated by white arrow was scanned by optical coherence tomography (OCT) (see **c**). **(b)** Fluorescein angiography (FAG) appearance at late phase. Mild hyperfluorescence is noted, suggesting CNV although there is no dye leakage. Center of lesion was horizontally scanned by OCT (black arrow). **(c)** OCT image. In lesion, highly reflective area colored white is continuous with retinal pigment epithelium (RPE) and appears as partial nodular thickening (white arrow). White bar: 250 μm . **(d)** Histopathology of same site. Rupture of Bruch's membrane and flat dome-like cell proliferation (white arrow) under retina can be seen. Proliferating cells consist mainly of immature vascular endothelial cells that have not formed lumen and less-pigmented, spindle-shaped RPE cells. White bar = 100 μm .

thalmoscopy (Figure 1a). On FAG, these lesions showed weak hyperfluorescence, suggesting the beginning of CNV (Figure 1b).

At the lesion, OCT imaging showed highly reflective areas that were displayed as white areas (Figure 1c). The reflex of these areas continued from the highly reflective layer corresponding to RPE/choriocapillaris and showed partial nodular thickening.

Histopathologically, these lesions showed rupture of Bruch's membrane with a low dome-like mound of proliferated cells in the subretinal space (Figure

1d). The cells consisted mainly of immature vascular endothelial cells and less-pigmented, spindle-shaped RPE cells. Formation of the vascular lumen was incomplete, and the intercellular space in the neovascular tissue was very narrow.

Active stage of CNV

In the active stage, fundus examination revealed irregularly round CNVs that appeared grayish- to yellowish-white, with clear borders under the retina

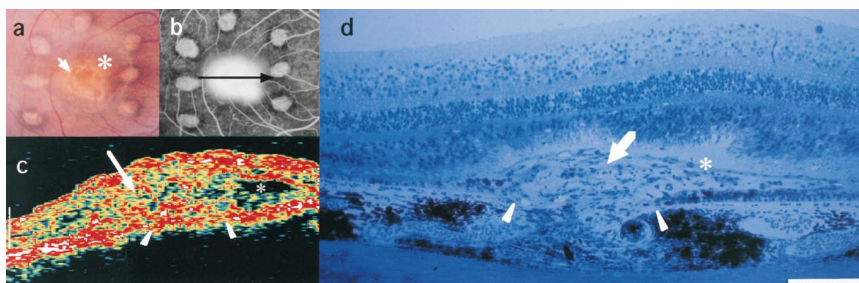


Figure 2. Active stage of choroidal neovascularization (CNV), 13 weeks after photocoagulation. **(a)** Color fundus photograph. Grayish white CNV with clear border is observed under retina (white arrow). At periphery of lesion, serous retinal detachment can be observed (*). **(b)** Fluorescein angiography. Marked dye leakage from CNV in late stage can be seen. Center of lesion was horizontally scanned by optical coherence tomography (OCT) (black arrow). **(c)** OCT image. Disruption of highly reflective layer corresponding to retinal pigment epithelium (RPE) can be seen (arrowheads). Multi-layered reflex, colored red, was observed under sensory retina (white arrow). At periphery of lesion, optical clear space corresponding to serous retinal detachment can be seen (*). White bar = 250 μm . **(d)** Histopathological study of same site. Bruch's membrane is disrupted (arrowheads) and well-developed CNV under sensory retina can be seen (white arrow). This corresponds with multi-layered reflex seen by OCT. CNV with wide lumens and less pigmented spindle RPE cells can be seen passing through rupture of Bruch's membrane. Intercellular spaces in CNV membrane are wide, and cell density is low. Accumulation of subretinal fluid is noted corresponding to optical clear space observed by OCT and retinal detachment by ophthalmoscopy (*). CNV is incompletely enveloped by RPE cells. White bar = 100 μm

(Figure 2a). At the periphery of the lesion, serous retinal detachment was detected.

On FAG, the CNV showed a lacy hyperfluorescence in the early phase, and a classic fluorescein angiographic pattern of marked dye leakage in the late phase (Figure 2b).

On OCT examination, a break in the highly reflective layer corresponding to the RPE/choriocapillaris was noted (Figure 2c). At these sites, a thick, multi-layered reflex area which was imaged as red was observed under the sensory retina. An optical clear space corresponding to serous retinal detachment was seen around these lesions corresponding to the serous detachment seen ophthalmoscopically.

In histopathological studies these lesions showed a rupture of Bruch's membrane and a well-developed CNV membrane under the sensory retina (Figure 2d). Neovascularization with wide vascular lumens had developed in the subretinal space at the site of rupture of Bruch's membrane. At the periphery of these lesions, proliferation of less-pigmented, spindle-shaped RPE cells was observed. The intercellular spaces were wide, and the cell density of the CNV membrane was low. There was incomplete envelopment of the CNV by RPE cells. The accumulation of subretinal fluid corresponding to retinal detachment was noted above the CNV membrane. These lesions were seen to consist of the CNV membrane developing above the RPE and passing into the sensory retina. Thus, this active stage of CNV was classified as Gass type 2 CNV in which the neovascularization progresses from below the RPE.

Regressive Stage of CNV

In the regressive stage, the CNV showed cicatrization with slight brown pigmentation on fundus examination (Figure 3a). The retinal detachment around the lesions was no longer present. The dye leakage in FAG was completely stopped, although the CNV was hyperfluorescent with dye staining (Figure 3b).

The OCT imaging showed a dome-shaped, highly reflective layer continuous with the reflectivity from the RPE and a moderately or highly reflective area under this layer (Figure 3c). No optical clear space was detected suggesting the recovery of the retinal detachment.

Histopathological studies of these sites revealed that the CNV that had grown through the rupture in Bruch's membrane was completely enveloped by monolayered, cuboidal-shaped RPE cells with melanin granules (Figure 3d).

OCT Images During the Course of CNV Stages of the Same Lesion

We were able to follow some of the CNVs from the active to the regression stage by these different techniques. During the active stage, fundus examination revealed a round grayish-white CNV with irregular edges and serous retinal detachment at the periphery of the lesions.

An example of this progression is shown in Figure 4. In the active stage, a multi-layered high reflex area (Figure 4a) was observed in the subretinal space as a red-colored area by OCT. The sensory retina was

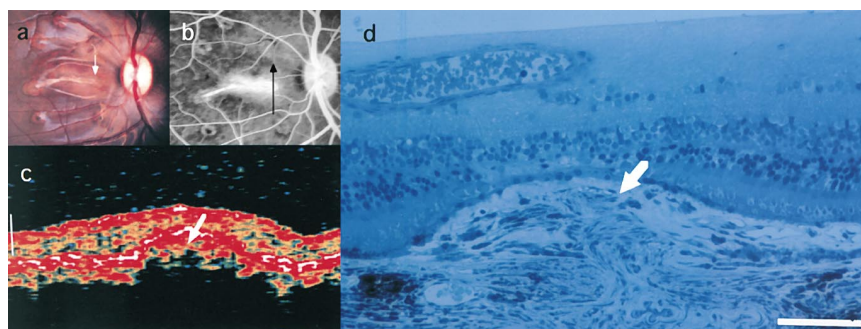


Figure 3. Regressive stage of choroidal neovascularization (CNV), 4 weeks after photocoagulation. (a) Color fundus photograph. Combined CNV is seen as cicatrized lesion under sensory retina (white arrow). (b) Fluorescein angiography. Late stage dye leakage from this lesion has completely stopped, although CNV is hyperfluorescent. CNV was scanned by optical coherence tomography (OCT) coronally (black arrow). (c) OCT image. Highly reflective layer colored white is continuous with retinal pigment epithelium (RPE) and shows dome-like thickening. Under this area, moderate or highly reflective areas are observed (white arrow). White bar = 250 μm . (d) Histopathological study of same site. White arrow: regressive CNV. CNV, which involved disrupted Bruch's membrane and subretinal region, is completely enveloped by monolayer of RPE cells with melanin pigment. White bar = 100 μm .

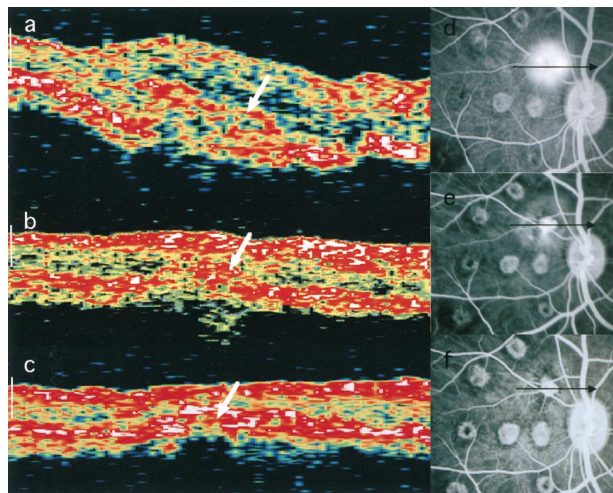


Figure 4. Course of choroidal neovascularization (CNV) regression in same lesion. Black arrow on fluorescein angiography (FAG): scan range of optical coherence tomography (OCT). White bar = 250 μm . (a) OCT image in active stage of CNV 2 weeks after photocoagulation. Multi-layered reflective layer colored red is seen (white arrow). Sensory retina shows thickening with diffuse low reflex. (b) OCT image in intermediate phase between active and regressive stage of CNV 4 weeks after photocoagulation. A stronger reflectivity of the CNV is observed than in active stage (white arrow). This layer continued smoothly from the highly reflective layer colored white corresponding to retinal pigment epithelium (RPE). Thickening of sensory retina is decreased. (c) OCT image in the regressive stage of CNV 13 weeks after photocoagulation. Highly reflective layer colored white is continuous with RPE and shows dome-like thickening. Under this area, moderate or highly reflective areas are observed (white arrow). (d) FAG in active stage of CNV 2 weeks after photocoagulation. Marked late stage dye leakage from CNV is present. (e) FAG in intermediate stage of CNV 4 weeks after photocoagulation. FAG reveals hyperfluorescence of CNV and late stage dye leakage is reduced. (f) FAG in regressive stage of CNV 13 weeks after photocoagulation. Late stage dye leakage from lesion has completely stopped, although CNV is hyperfluorescent.

thickened corresponding to the edema seen by ophthalmoscopy. Between the active and regressive stages of this lesion, the reflectivity (Figure 4b) was higher than that during the early active stage, and the reflectivity changed smoothly to the highly reflective RPE layer. The thickening of the sensory retina was decreased. In the regressive stage, the dome-like elevation of whitish reflective layer corresponding to the RPE was observed. Under this layer, a moderate reflex area colored red to yellow was observed (Figure 4c).

In the active stage, FAG revealed marked dye leakage from the neovascularization (Figure 4d).

During the course of the active stage, fundus examination revealed a decrease in the serous retinal detachment. Although FAG revealed hyperfluorescence of the CNV, dye leakage was reduced in the intermediate stage (Figure 4e). During the regressive stage, the CNV showed cicatrization with slight brown pigmentation. The dye leakage in FAG was completely stopped although the CNV was hyperfluorescent in the regressive stage (Figure 4f).

Active CNV with a Subretinal Hematoma

In one of the lesions, fundus examination revealed a red to partially yellow subretinal hematoma. A grayish-white CNV was observed in and below the subretinal hematoma. There was extensive serous retinal detachment and marked edema in the periphery of the lesion. FAG revealed late dye leakage from the CNV and the blockage of the leakage over the hematoma.

This site including the hematoma was scanned by OCT. The sensory retina at the site of the hematoma showed a dome-like elevation. The reflex of the sensory retina was enhanced, demonstrating a thick, highly reflective layer. Under the retinal layers, the subretinal neovascular tissues were not detected due to the reduction of the scattered light by the hematoma.

Histopathological study of this lesion showed the dome-shaped hematoma composed of tightly packed erythrocytes under the retina. Neovascular membranes that were rich in fibrous connective tissues were present in the subretinal space.

Discussion

The standard diagnostic imaging methods for obtaining tomographic images of human eyes include x-rays, computed tomography, magnetic resonance imaging, and ultrasonography. In addition, the recent development of an ultrasound biomicroscope has facilitated the detection of pathological changes of the anterior segment of the eye at a resolution value of 20 μm with high frequency ultrasound.

Optical coherence tomography imaging utilizes the interference of light phenomenon and is useful for the examination of the fundus. Because the speed of light is approximately 10^6 -fold faster than that of sound waves, the axial resolution is extremely fine and fundus lesions can be detected at a resolution of 10 μm . This resolution is comparable to that for light microscopes.

There have been previous studies comparing OCT images to histopathological findings in animals^{10–12}

although there are some problems in comparing the two types of images. In histology, specimens are fixed, dehydrated and embedded, and cellular components are examined after staining. During these procedures, tissue contraction and distortion usually occur. In the OCT images, absorption, scatter, and diffraction of the light rays may affect the tomographic images. In addition, OCT images can be easily altered by pigments such as melanin and hemoglobin. Thus, comparisons of the two types of images must be done, taking these artifacts into consideration.

Earlier, Toth et al¹¹ photocoagulated monkey eyes with a laser and compared the OCT images of the photocoagulated regions of the retina to the histological appearance in the same regions. They reported that the tomographic images correlated well with the light microscopic findings, suggesting the usefulness of OCT in spite of the limitations discussed.

Similarly, we have compared OCT and histopathological images of experimental CNV tissues, which has not been done in any previous studies. Our results also showed that the OCT images of CNVs correlated well with the histopathological findings, suggesting that OCT imaging can be useful in determining not only the shape and locus of the CNVs but also in predicting the cellular make-up of the tissue involved in the CNVs.

There have been studies that report the OCT findings of CNV in patients. Hee et al³ classified the OCT findings of AMD into five categories: (1) well-defined CNV, (2) poorly defined CNV, (3) serous pigment epithelial detachment, (4) fibrovascular pigment epithelial detachment, and (5) hemorrhagic pigment epithelial detachment. They reported that OCT imaging had revealed fibrovascular pigment epithelial detachment in some exceptional cases, even though FAG had shown the typical findings of a well-defined CNV. In our experimental model, none of the animals showed pigment epithelial detachment, but CNV findings of type 1 and type 2 were observed serially.

Puliafito et al⁶ reported that the site of the CNV, originating either beneath the retina or beneath the RPE, could be differentiated by OCT. Similarly, Giovannini et al¹⁴ also reported that the position of the neovascularization relative to the RPE could be differentiated by OCT, and indicated that OCT was useful in patients with exudative AMD. In our experiment, the active stage of CNV was identified as having the properties of a Gass type 2 neovascularization in which the neovascularization progresses from below the RPE.

Although this experimental model is essentially different from the model of type 1 neovascularization because of the difference between the regenerated RPE and native RPE, the CNV enveloped by the RPE at the regressive stage is valuable as a lesion that resembles a Gass type 1 neovascularization for the reason that we can observe the CNV lying below the RPE by OCT.

In this study, examination of OCT findings during the developmental, active, and regressive stages confirmed that the tissue composition of the CNV could be determined by OCT. During the developmental stage, compact CNV tissue, composed mainly of immature new vessels and proliferated RPE cells, in our histopathological study could be observed by OCT as a nodular reflex area colored white with high reflectivity. OCT imaging demonstrated changes in the lesion that could not be detected by standard FAG examination. In addition, OCT imaging has raised the possibility of detecting the CNV at the time when a blood vessel's cavity is immature.

Active lesions of Gass type 2 neovascularization were revealed as multi-layered reflex areas colored red with peripheral optical clear spaces related to retinal detachment. Histopathologically, differences between the active stage and the developmental stage as described may consist of the size of neovascularization lumens and the density of cells composing the CNV membrane.

In regressive lesions, envelopment of CNV by RPE was observed by OCT as a low, dome-like, white reflective layer continuous from the high reflective RPE layer. These observations were consistent with the histopathological findings. Beneath such dome-shaped, high reflex area, a moderate reflective area was observed. The reflectivity of the CNV enveloped by RPE was imaged as a lower reflex compared to the usual active CNV, because of the scattering caused by the enveloping RPE. In CNV with subretinal hematoma, a large volume of erythrocytes accumulated under the retina to reduce the reflex by scattering, and neovascularization in the deep layer could not be imaged.

In summary, OCT has been shown to facilitate the imaging of the sensory retina and RPE in the eyes of experimental animals. The positional relationship between neovascularization and RPE could be clearly revealed by OCT. However, it may be difficult to detect small or even larger flat lesions due to the resolution and distortions induced by overlying tissue. Optical coherence tomography may be useful for distinguishing type 1 from type 2 CNV by their tomographic appearance. In the future, OCT com-

bined with FAG or ICG may be used in deciding to treat, and the course of surgery for, neovascular maculopathy, including exudative AMD.

References

1. Huang D, Swanson ER, Lin CP, et al. Optical coherence tomography. *Science* 1991;254:1178–81.
2. Hee MR, Izatt JA, Swanson EA, et al. Optical coherence tomography of the human retina. *Arch Ophthalmol* 1995;113:325–32.
3. Hee MR, Bauman CR, Puliafito CA, et al. Optical coherence tomography of age-related macular degeneration and choroidal neovascularization. *Ophthalmology* 1996;103:1260–70.
4. Izatt JA, Hee MR, Swanson EA, et al. Micrometer-scale resolution imaging of the anterior eye in vivo with optical coherence tomography. *Arch Ophthalmol* 1994;112:1584–9.
5. Puliafito CA, Hee HR, Lin CP, et al. Imaging of macular diseases with optical coherence tomography. *Ophthalmology* 1995;102:217–29.
6. Puliafito CA, Hee HR, Schuman JS, Fujimoto JG. Optical coherence tomography of ocular diseases. Thorofare, NJ: Slack Inc., 1996:3–15.
7. Yannuzzi LA, Slakter JS, Sorenson JA, Guyer DR, Orlock DA. Digital indocyanine green videoangiography and choroidal neovascularization. *Retina* 1992;12:191–223.
8. Yannuzzi LA, Hope-Ross M, Slakter JS. Analysis of vascularized pigment epithelial detachments using indocyanine green videoangiography. *Retina* 1994;14:99–113.
9. Gass JDM. Biomicroscopic and histopathologic considerations regarding the feasibility of surgical excision of subfoveal neovascular membranes. *Am J Ophthalmol* 1994;118:285–98.
10. Huang Y, Cideciyan AV, Papastergiou GI, et al. Relation of optical coherence tomography to microanatomy in normal and rd chickens. *Invest Ophthalmol Vis Sci* 1998;39:2405–16.
11. Toth CA, Birngruber R, Boppart SA, et al. Argon laser retinal lesions evaluated in vivo by optical coherence tomography. *Am J Ophthalmol* 1997;123:188–98.
12. Toth CA, Narayan DG, Boppart SA, et al. A comparison of retinal morphology viewed by optical coherence tomography and by light microscopy. *Arch Ophthalmol* 1998;115:1425–8.
13. Ryan SJ. Subretinal neovascularization. Natural history of an experimental model. *Arch Ophthalmol* 1982;100:1804–9.
14. Giovannini A, Amato GP, Mariotti C, Scassellati-Sforzolini B. OCT imaging of choroidal neovascularization and its role in the determination of patients' eligibility for surgery. *Br J Ophthalmol* 1999;83:438–42.